

Quantifying the Effect of Guest Binding on Host Environment

Hugh P. Ryan, Zachary S. Fishman, Jacob T. Pawlik, Angela Grommet, Malgorzata Musial, Felix Rizzuto, James C. Booth, Christian J. Long, Kathleen Schwarz, Nathan D. Orloff, Jonathan R. Nitschke, and Angela C. Stelson*



Cite This: *J. Am. Chem. Soc.* 2023, 145, 19533–19541



Read Online

ACCESS |



Metrics & More

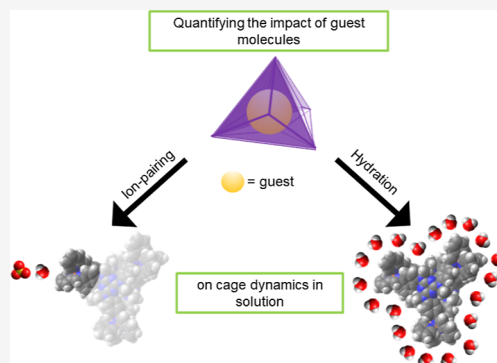


Article Recommendations



Supporting Information

ABSTRACT: The environment around a host–guest complex is defined by intermolecular interactions between the complex, solvent molecules, and counterions. These interactions govern both the solubility of these complexes and the rates of reactions occurring within the host molecules and can be critical to catalytic and separation applications of host–guest systems. However, these interactions are challenging to detect using standard analytical chemistry techniques. Here, we quantify the hydration and ion pairing of a $\text{Fe}^{\text{II}}_4\text{L}_4$ coordination cage with a set of guest molecules having widely varying physicochemical properties. The impact of guest properties on host ion pairing and hydration was determined through microwave microfluidic measurements paired with principal component analysis (PCA). This analysis showed that introducing guest molecules into solution displaced counterions that were bound to the cage, and that the solvent solubility of the guest has the greatest impact on the solvent and ion-pairing dynamics surrounding the host. Specifically, we found that when we performed PCA of the measured equivalent circuit parameters and the solubility and dipole moment, we observed a high (>90%) explained variance for the first two principal components for each circuit parameter. We also observed that cage-counterion pairing is well-described by a single ion-pairing type, with a one-step reaction model independent of the type of cargo, and that the ion-pairing association constant is reduced for cargo with higher water solubility. Quantifying hydration and cage-counterion interactions is a critical step to building the next generation of design criteria for host–guest chemistries.



INTRODUCTION

Molecular self-assembly facilitates the construction of a diverse array of complex supramolecular architectures from simple building blocks.¹ Among these architectures, metal–organic cages attract significant interest due to their ability to encapsulate and stabilize molecular cargoes in water.² Quantitative studies of the host–guest chemistry of these cages^{3,4} have shown that factors such as the hydrophobic effect and the physicochemical properties of the guest species are key to understanding these encapsulation phenomena. Furthermore, the hydrophobic spaces defined by metal–organic coordination cages have been exploited to achieve chemical separations⁵ and to favor molecular conformations that enable new catalytic reactions.^{6,7}

While there are extensive studies of intermolecular interactions within the cavity, there is growing recognition that the environment outside of the cage, that is interactions involving solvent molecules and counterions, can exert a strong influence over the system-wide behavior of these complexes.⁸ Counterions often serve as templates for self-assembly of the cage framework and achieving fast counterion displacement kinetics is critical to designing cages that are sufficiently dynamic to support guest exchange for applications including catalysis.⁸ Beyond the cage assembly, the choice of counterion

can also be critical. One recent study demonstrated that the choice of counterion had a direct effect on the rate of a Kemp elimination reaction within a cubic metal–organic coordination cage.⁶ Another showed that the choice of anion and degree of anion exchange tuned the solubility of cages in solution and allowed phase transfer between solvents.⁹ Other studies have shown that the choice of counterion can affect additional properties and phenomena such as solubility¹⁰ and hierarchical self-assembly.¹¹ Currently, knowledge is limited to the interactions of counterions with the cavity and cage as a whole.

While it is apparent that solvation and ion-pairing are of pivotal importance in the study of metal–organic coordination cages, these effects are not typically measured due to the difficulty in detecting these nonspecific interactions via standard analytic techniques such as NMR (nuclear magnetic

Received: February 9, 2023

Published: August 29, 2023



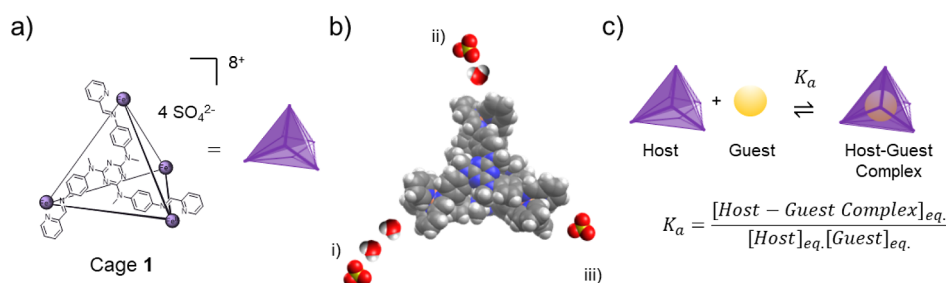


Figure 1. Chemical model of cage 1 (a) and space-filling model (b) with illustrated ion pair configurations (i: double solvated, ii: single solvated, iii: contact ion pair, ion is depicted as orange circle). (c) We assume the host cage and guest molecule are in equilibrium with the host–guest complex with associated equilibrium constant K_a . We selected guest molecules with high K_a that are more strongly bound to the cages.

resonance) spectroscopy, calorimetry, and optical spectroscopy. In contrast, microwave dielectric spectroscopy is a particularly promising technique for gauging ion-pairing interactions and has been applied to investigations of biomolecules^{12,13} and of ion dynamics in salt solutions.^{14–16} Microwave dielectric spectroscopy measures the complex (real and imaginary) permittivity of a solution as a function of frequency in the microwave range (kilohertz to approximately 100 GHz). Among other things, the frequency-dependent complex permittivity captures information about the responses of the dipoles in solution, including the dipoles of ion pairs and the hydrogen bonding network of water. Microwave microfluidic spectroscopy (MMS, an on-chip variety of microwave dielectric spectroscopy) has been used to study the ion-pairing of two metal–organic coordination cages in water in the absence of molecular guests.¹⁷ However, this technique has not been applied to quantify the solvation and ion-pairing states of a metal–organic coordination cage as a function of molecular cargo.

Here, we use MMS to investigate how different molecular guests alter the interactions of a metal–organic coordination cage with its external environment. Specifically, we measure the broadband dielectric responses of metal–organic coordination cages in solution as a function of concentration and guest species. The dielectric response of the cage solution includes equivalent circuit parameters related to the mobility of ions in solution, the ion-pairing of the cages, and the solvation of the cages. To quantify the relationship between the equivalent circuit parameters and the physicochemical properties of the guests, we perform principal component analysis (PCA) on the equivalent circuit parameters evaluated as a function of cage concentration. Overall, we found that the key physicochemical properties of the guest that describe the solvation and ion-pairing environment of the cage are the solubility of the guest and its dipole moment. Specifically, we found that when we performed PCA of the equivalent circuit parameters and the solubility and dipole moment, we observed a high (>90%) explained variance for the first two principal components for each circuit parameter. Taken as a whole, these analyses point to the strong but complicated relationship between guest solubility and nonspecific interactions with the cage. Elucidating the impact of the guest on the cage dynamics in solution helps future designs of systems of metal–organic coordination cages and their molecular guests for novel applications in molecular separations and catalysis.

The host–guest chemistry of metal–organic cages has been studied extensively.¹ We selected cage 1 (see Figure 1, Supporting Information for more details) as a good candidate for this study because it has already been shown to encapsulate

a range of aliphatic and aromatic hydrocarbons, up to the size of adamantane derivatives, in water and acetonitrile.¹⁸ These encapsulation phenomena can be described by a simple 1:1 binding model, in which one cage and one molecule of cargo form a host–guest complex (Figure 1c).

For this study, we selected a range of guest molecules that vary across several physicochemical properties, including dipole moment, volume, polarizability, and hydrophobicity. The complete list of guests is listed in Table 1, along with the

Table 1. List of the Investigated Guest Molecules and Their Relevant Molecular Descriptors for PCA (See Supporting Information for More Details)

	solubility (mg/L)	logP	dipole moment (D)
fluoroadamantane	38.19	3.84	1.9656
cyclohexane	55	3.18	0
2-hexylthiophene	4.831	4.82	0.7626
methylcyclopentane	49.37	3.10	0.067
1-methyladamantane	3.912	4.39	0.0916
naphthalene	142.1	3.17	0
tetrahydrofuran	54,480	0.94	1.7883
mesitylene	120.3	3.63	0.0878
pyridine	729,800	0.80	2.184

logarithm of their octanol–water partition coefficients (logP), water solubilities, and dipole moments. The water solubility and the logarithm of the octanol–water partition coefficient are both metrics of water solubility, but the logarithm scale of the partition coefficient provides a transformation that allows poorly soluble guests to be more distinguishable for the PCA. We performed comparisons of logP and water solubility PCA analyses and found that in some cases, the variance was slightly better explained by the water solubility on a linear scale, and this warrants consideration to motivate future studies of more water-soluble guests. In the way that these studies are performed, there is no input duplication for the PCA, since each analysis is performed on two measurands (slope and intercept of an equivalent circuit parameter) and a single chemical property. The complete table of physicochemical properties included in this study is found in Supporting Information Table 1. For each cargo, uptake into the cage cavity was verified with NMR studies (Supporting Information).

RESULTS AND DISCUSSION

Microwave measurements of cage solutions reveal a complex set of interrelated equivalent circuit parameters that are impacted by the solvation and ion-pairing states of the cage.

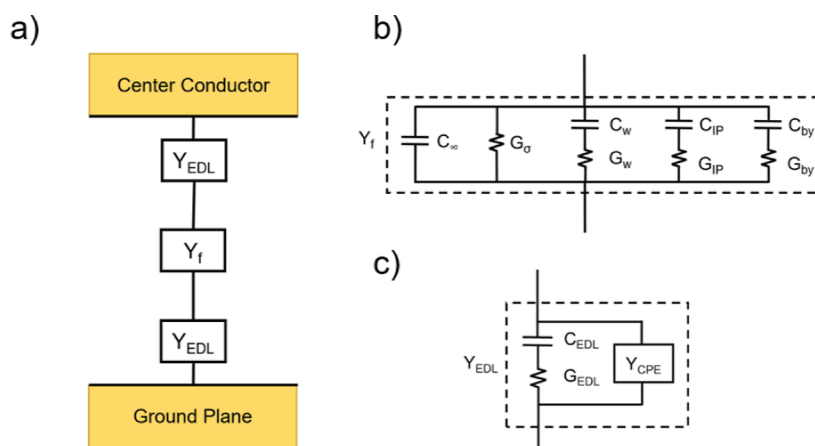


Figure 2. Circuit model for 1 species in solution with and without guest species. (a) Total fluid admittance is comprised of the electrical double layer (EDL) admittance Y_{EDL} in series with the fluid bulk admittance Y_f . (b) Equivalent circuit model of Y_f where C_∞ is the capacitance at frequencies higher than the measurements performed here, G_σ is the conductance due to ions, C_w , G_w , C_{IP} , G_{IP} , C_{by} and G_{by} are the equivalent capacitances (C) and conductance (G) of the Debye relaxations in the bulk fluid (water, w ; cage ion pair, IP ; and byproduct $FeSO_4$ ion pairing, by). (c) Equivalent circuit of Y_{EDL} , where Y_{CPE} is the admittance of the constant-phase element (CPE), and C_{EDL} and G_{EDL} represent the Debye relaxation form of the EDL.

Since equivalent circuit parameters are core to this analysis, we define them here. In dielectric measurements of fluids and materials, it is possible to construct a circuit model that is electrically equivalent to the properties of the material itself. We use these circuit models to fit MMS spectra, and the fitted circuit parameters can be used to extract kinetic and thermodynamic quantities of charged species in solution.¹⁹ These equivalent circuit models can contain Debye relaxations (modeled as resistor-capacitor elements), conduction mechanisms (modeled as resistors), and interfacial effects.²⁰ We begin by showing the impact of different cargos on the most relevant equivalent circuit parameters and explaining the relationship between the circuit parameter and the environment of the cage.

While the full equivalent circuit model of the cage solution contains many elements (Figure 2), we limit our discussion to those associated with the behavior of cages in solution and refer the reader to the Supporting Information for the full equivalent circuit model data set. For each equivalent circuit parameter we consider, we show the fitted frequency-dependent contribution of that circuit element (black square dots) and the data associated with that component of the fitting (light blue line) in Figures 4a, 5a, and 6a. To calculate the data associated with a given equivalent circuit element, we calculate the capacitance and conductance of an equivalent circuit model that does not include the element and subtract this from our data. The resulting values include the noise in the data and the portion of the data not explained by other equivalent circuit parameters. This method of isolating the different parts of the data helps diagnose overfitting and systematic deviations in fitting in complex equivalent circuit models. We show the extracted fit parameter as a function of the cage concentration and cargo with associated uncertainties in the fit. For a more complete discussion of the measurement uncertainties, see the Uncertainty Assessment in the Supporting Information.

For each PCA analysis, we show a score plot of the cargo data point for the first two principal components. These score plots are primarily used to identify outliers in the data as the sample size is not large enough to identify distinct populations within the data. To quantify the relationship between the

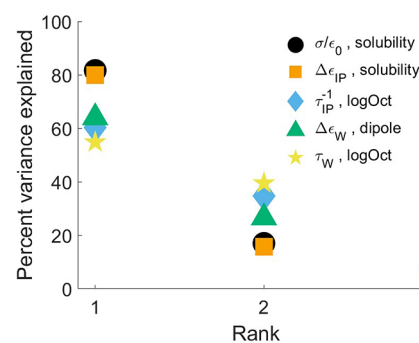


Figure 3. Percent variance captured by the first three principal components of the PCA calculations for each equivalent circuit parameter combined with a single chemical property taken from Table 1. In the legend, solubility indicates water solubility, logP indicates the logarithm of the octanol–water partition coefficient, dipole indicates dipole moment, σ is the ionic conductivity, $\Delta\epsilon_{IP}$ is the permittivity decrement due to ion pairing, τ_{IP} is the time constant of the ion pairing relaxation, $\Delta\epsilon_w$ is the permittivity decrement due to the water relaxation, and τ_w is the time constant of the water relaxation.

physicochemical properties of the guest and the electrical phenomena in solution, we applied PCA to a subset of our results. PCA is a method of analyzing complex data sets, where the data cannot be readily decomposed into independent uncorrelated variables. This data complexity is true for MMS spectra, where several equivalent circuit elements are dependent on the presence of ion pairs. Furthermore, we expect guest properties to be correlated as well—for example, volume and surface area. For each PCA analysis, we included one chemical property and the slope and intercept of each equivalent circuit parameter as a function of concentration. We calculated the slopes and intercepts with the York linear fitting algorithm.²¹ Fitting results are shown in Figures 4–6. For each of the PCA results, we calculated the variance described by the principal components (Figure 3). In all cases presented here, more than 90% of the variance in the measurand and chemical properties was captured by the first two principal components, indicating a strong correlation between the measurands and the

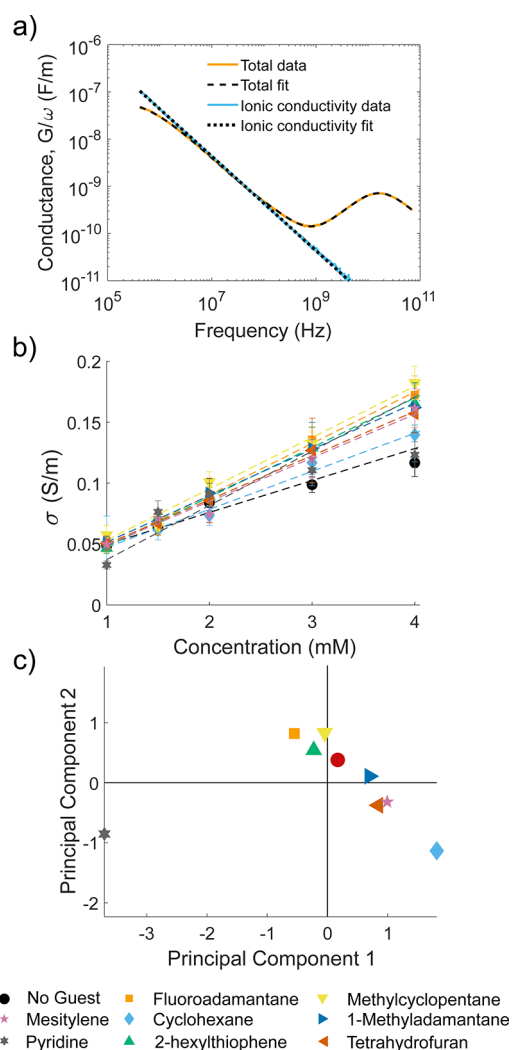


Figure 4. (a) Contribution of free ions to conductance in MMS conductance spectra. The yellow line is the full spectrum, and the black dashed line is the full equivalent circuit model fit. The data associated with the ionic conductivity (σ) are plotted in blue, and the black dotted line is the fit associated with σ . (b) Ionic conductivity as a function of concentration of cages with no cargo (black) and loaded with different cargo. Dotted lines provide a fit for each data set. (c) Score plot of all samples represented by the first two principal components, consisting of linear combinations of ionic conductivity slope, ionic conductivity intercept, and water solubility.

physicochemical properties. To perform an outlier analysis on our PCA analysis, we first generated the components and examined the scores of each guest data set. We then removed the set of data which had the largest score on the first principal component and reperformed the PCA to ensure that the variance was still well explained by the chemical property. The data presented here includes outliers.

Ionic Conductivity. MMS probes the ionic conductivity of a solution. The contribution of the ionic conductivity equivalent circuit element to the measured conductance has the form²⁰

$$\frac{G_{\sigma}}{\omega} = \frac{\sigma}{k_{\text{geom}}} \quad (1)$$

(see Figure 4a), where G_{σ} is the conductance due to ions, ω is the angular frequency, σ is the ionic conductivity and k_{geom} is a

geometric factor that relates the measured quantities to the bulk properties of the fluid. We calculate k_{geom} for each microwave microfluidic device from measurements of samples with known permittivities (air, relative permittivity $\epsilon_r = 1.00$, and D_2O , $\epsilon_r = 77.94$, see eqs 2 and 3). The ionic conductivity of a solution is determined by the concentrations, mobilities, and lifetimes of ionic species in solution. In simple salt solutions, ionic conductivity can be used to directly calculate the concentration of ion pairs;¹⁴ however, this calculation is not possible in a solution of a metal–organic cage, where the mobilities of charged species in solution are not readily calculated and many charged species may exist.

Here, we compared the change in the ionic conductivity as a function of cage concentration in solution. This approach allows us to compare the population of free ions in solution as a function of guest without directly calculating the ion pair concentrations. Because we observe a linear dependence of ionic conductivity upon cage concentration and all species in solution are strong electrolytes, we infer that the mobilities of the charged species in bulk solution remain independent of cargo and that all changes observed are due to the changes in free ion concentration in solution. This inference simplifies the system as the effective mass of the cage will change only slightly with different guests. However, we anticipate that the cage mobility overall is much lower than that of the counterions, and previous NMR studies of this cage with different guests showed diffusion coefficients very similar for the various cage–guest complexes. For example, we calculated a diffusion coefficient of $1.59 \pm 0.01 \times 10^{-10} \text{ m}^2/\text{s}$ for a cage without guest, $1.63 \pm 0.02 \times 10^{-10} \text{ m}^2/\text{s}$ for a cage with 1-methyladamantane, and $1.62 \pm 0.02 \times 10^{-10} \text{ m}^2/\text{s}$ for a cage with 1-methylcyclopentanone (see Supporting Information, NMR Methods Section). Reference 18 shows the diffusion coefficients of several other cargo that are also quite similar.

We observe that the sample with no guest has the smallest slope in ionic conductivity as a function of cage concentration compared to all samples with guests bound (Figure 4b). This observation implies that cage-counterion pairing is reduced by the introduction of a guest, regardless of guest identity. We infer this reduction to result from displacement of counterions from the cage cavity by guest molecules. This conclusion is supported by X-ray crystallography of cage systems that often show counterions in the cage cavity, as well as studies of NMR-active counterions that bind to cages in solution.²⁰ We observed nonlinear ionic conductivity with pyridine as a guest, which we attribute to coordination between excess pyridine in solution and the excess iron(II) sulfate left over from cage assembly. In separate experiments, we observed the formation of a pale brown precipitate from aqueous solutions of iron(II) sulfate and pyridine, supporting our hypothesis. Oligomeric structures of pyridine–sulfate complexes have been observed in the literature,²² which could also account for the anomalous properties of the pyridine samples. PCA analysis of the ionic conductivity (Figure 4c) showed that the ionic conductivity was described well by including water solubility as a chemical property in the PCA analysis. Pyridine is an outlier in this PCA analysis score plot in Figure 4c and in the ionic conductivity data as a function of concentration. Excluding this pyridine data, there is a good correlation in the logarithm of the octanol/water partition coefficient, and the score plot shows the other cargoes clustered into a single population. Independent of the behavior of the pyridine, this finding suggests that the amount of free ions (i.e., unbound to the

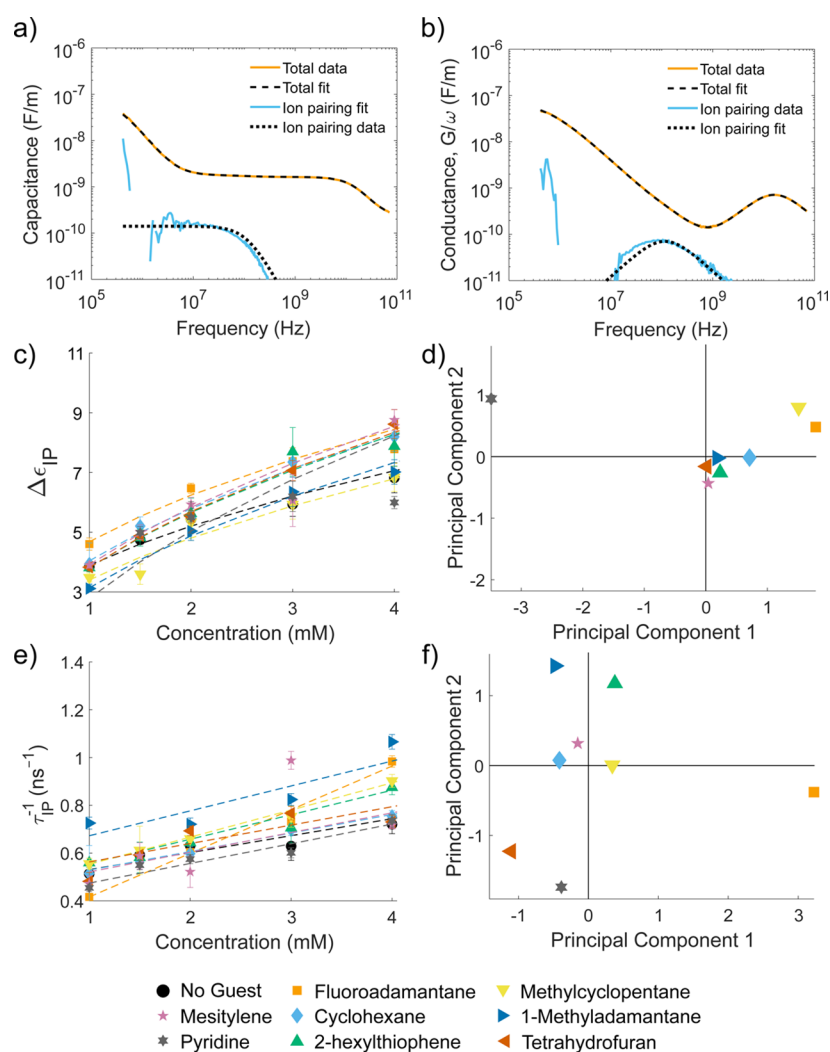


Figure 5. (a) Contribution of cage-counterion pair Debye relaxation to (a) MMS capacitance spectra and (b) MMS conductance spectra. For (a,b), the full spectra are in yellow, and the black dashed lines provide full equivalent circuit model fits. The data associated with the Debye relaxation are colored blue, and the black dotted lines are the fits associated with the ion-pairing Debye relaxation. (c) Permittivity contribution $\Delta\epsilon_{IP}$ and (e) ion pairing time constant τ_{IP} as a function of cage concentration for cages with no guests (black) and loaded with different cargo. Dotted lines are the fit of each data set. (d,f) Score plot of all samples represented by the first two principal components consisting of linear combinations of (d) $\Delta\epsilon_{IP}$ slope, intercept, and water solubility and (f) τ_{IP} slope, intercept, and the logarithm of the octanol–water partition coefficient.

host) in solution is most closely correlated to the aqueous solubility of the guest.

Debye Relaxations. In the cage solutions we measure here, there are 2 equivalent circuit elements that are associated with the cage environment in solution: one is due to the cage-counterion pair dipole, and the other describes the response of the hydrogen bonding network of the water to the applied electric field.^{23–25} These circuit elements are described by Debye relaxations that are caused by the dipoles in solution responding to the electric field. In our spectra, Debye relaxations are characterized by their magnitude ($\Delta\epsilon$, enhancement of permittivity relative to free space) and a time constant (τ)²⁰

$$\epsilon(\omega) = \frac{\Delta\epsilon}{1 + (i\omega\tau)} \quad (2)$$

These quantities are related to the concentrations and kinetics of the dipoles in solution.²⁶ The contributions of these Debye relaxations to the measured capacitance and con-

ductance of the microfluidic measurements are listed in Figure 5a. The measured Debye relaxations can be converted to permittivity by the geometric factor k_{geom} , which can be calculated from measurements of the capacitance and conductance of the fluid-loaded device (C_f and G_f) and the capacitance of the empty device C_{air}

$$\epsilon' = (C_f - C_{air})k_{geom} + \epsilon_0 \quad (3)$$

$$\epsilon'' = \frac{G_f}{\omega} k_{geom} \quad (4)$$

Cage-counterion Relaxation. We observed that the dielectric decrement of $\Delta\epsilon_{IP}$ increases as a function of cage concentration nonlinearly in all cage samples (Figure 5c). This increase is consistent with other dielectric measurements of ion pairing in metal–organic cage samples, and we empirically fit the cage concentration dependence to a square-root function¹⁷

$$\epsilon''_{ions} = a\sqrt{[I]} + b \quad (5)$$

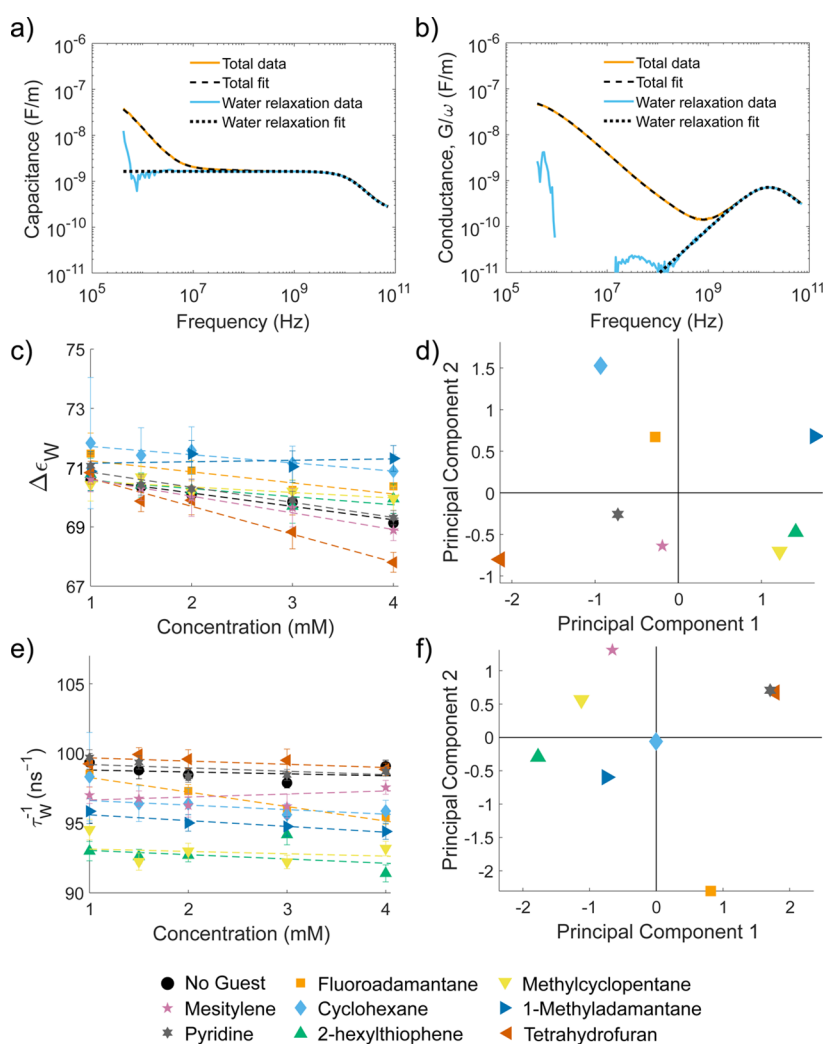


Figure 6. (a) Contribution of water Debye relaxation to (a) MMS capacitance spectra and (b) MMS conductance spectra. For (a,b), the full spectra are in yellow, and the black dashed lines are the full equivalent circuit model fits. The data associated with the Debye relaxation are in blue, and the black dotted line is the fit associated with the water Debye relaxation. (c) Permittivity contribution $\Delta\epsilon_W$ as a function of cage concentration for cages with no cargo (black) and loaded with different cargo. Dotted lines are the fit of each data set. (e) Water relaxation time constant τ_W . (d,f) Score plot of all samples represented by the first two principal components, consisting of linear combinations of (d) $\Delta\epsilon_W$ slope, intercept, and dipole moment and (f) τ_W slope, intercept, and the logarithm of the octanol–water partition coefficient.

where **1** is the cage species illustrated in Figure 1. For the “no guest” sample, we observe that $\Delta\epsilon_{IP}$ increases the least as a function of the cage concentration. In simple ion pair models, the permittivity decrement of the ion-pairing relaxation relates to the concentration of ion pairs in solution.²⁷ In other studies of ion pairs, a Clausius–Mossotti formulation has been used to calculate the concentration of ion pairs in solution.²⁷ This model assumes a simple, charge-balanced dipole consisting of point charges within an ellipsoid of a uniform dielectric constant. The Clausius–Mossotti formulation from ref 27 of the ion pair is likely insufficient to quantitatively describe the relationship between the dielectric decrement and the concentration of ion pairs in solution for this complex system with organic ligands because the polarizability and aspect ratio of the ion-pairing environment is not well-known. However, we use the general form of the modified Cavell equation²⁷ to inform our interpretation of the trends as a function of guest identity. In the case of the “no guest” sample, the smaller dielectric decrement as a function of cage concentration might be explained in three ways: (1) there were fewer ion pairs in

the cages with no guest; (2) the presence of cargo changed the polarizability of the ion pair environment; and (3) the presence of an SO_4^{2-} counterion in the center of the cage reduces the net dipole moment of the cage-counterion pairs. Given that the ionic conductivity results strongly suggested the presence of more bound ions when no guest is inside the cage, the first explanation is inconsistent with our findings. Cages with no guest are expected to contain several water molecules²⁸ within their cavities that we expect to have lower polarizability than the guest molecules used in this study. However, the impact of confined water molecules on the dielectric environment of the cage-counterion pair is difficult to predict due to the complex relationship between the hydrogen bonding state of water and its dielectric constant.²⁹

The slope and intercept of the $\Delta\epsilon_{IP}$ fit described above are best described by a PCA that includes the water solubility of the cargo. These findings show a trend similar to the PCA score plot of the ionic conductivity, where pyridine is an outlier and the less soluble guests are more clustered. However, similar to the case of ionic conductivity, the PCA is robust

against the exclusion of the pyridine sample, and the parameter that best describes the data set is the $\log(\text{octanol-water partition coefficient})$. We considered physicochemical properties that would describe the changes to the dielectric environment within the cage, including dipole moment and polarizability, and none of these properties resulted in a PCA with high explained variance. This finding detracts from the explanation whereby the changes in $\Delta\epsilon_{\text{IP}}$ due to cargo are primarily due to the polarizability of the cargo in the environment of the ion pair.

The time constant τ_{IP} of a Debye relaxation of an ion pair relates to the rotation and the pairing kinetics of the system.^{17,30} In a one-step reaction model, where a free counterion is bound to a vertex of the cage, the time constant depends linearly on the concentration of species in solution¹⁷

$$\frac{1}{\tau_{\text{IP}}} = \frac{1}{\tau_{\text{or}}} + k_{-1} + k_1(8[1] - 2[c_{\text{IP}}]) \quad (6)$$

where τ_{or} is the reorientation time constant of the ion pair, $[c_{\text{IP}}]$ is the concentration of ion pairs in solution, and k_1 and k_{-1} are the formation and decay rates of the ion pair, respectively. This relationship shows that the slope of the line is related to the formation rate of the ion pair, while the intercept is related to its decay and reorientation in response to the electric field. It is notable that the ion-pairing in these cage systems is adequately described by a single Debye relaxation, since simpler sulfate salts show multiple Debye relaxations associated with multiple ion-pairing states in solution.^{31,32} This finding has implications for the design of host-guest interactions, as it implies that there is one dominant ion-pairing interaction to consider in this cage system rather than many competing interactions with varying kinetics.

The ion pairing time constant is linear in all of the samples, indicating a single-step ion pairing reaction mechanism in all cases. Both the slope and the intercept vary with guest identity, and we observe a lower slope for samples with water-soluble guests or no guest molecules. This observation implies through eq 1 that ion pair formation is slower for water-soluble guests, and we hypothesize that the changes observed result from the more soluble guest more readily disassociating from the cage, interrupting cage-counterion pairing. In PCA, the logarithm of the octanol-water partition coefficient is the property that best describes the variance in the τ_{IP} slope and intercept. Notably, the PCA score plots for the water relaxation do not show the pyridine sample as an outlier in the population, indicating that the impact of pyridine binding does not substantially impact the solvation behavior of the cages. Together with the sigma and $\Delta\epsilon_{\text{IP}}$ PCA results, these findings point to the water solubility of the guest changing the cage and counterion behavior in solution. These findings demonstrate that the choice of guest affects not just the electrostatic environment of the cage, but the kinetics of the cage-counterion interaction.

D₂O Relaxation. The dielectric relaxation of D₂O molecules ($\Delta\epsilon_{\text{W}}$) [Figure 6a,b] dominated the dielectric spectra above 1 GHz. This relaxation phenomenon is well-characterized and has been used to estimate the number of bound water molecules per ion in simple systems.²⁷ In this system, the solvent relaxation is primarily due to D₂O molecules, but a small quantity of acetonitrile (less than 2%) remains in solution from the synthesis of the cages (see Supporting Information for more details on the acetonitrile characterization and synthesis procedure). For $\Delta\epsilon_{\text{W}}$, we observe two distinct populations as a function of guest (Figure

6c). The guests that are more soluble in water have overall lower magnitudes of water relaxation and steeper slopes, showing more similar behavior to the “no guest” case. Insoluble guests have higher water relaxation magnitudes, indicating less water is bound in the solvation shell of the cage. We attribute this observation to two phenomena: (1) the displacement of water inside the cage cavity by insoluble guests and (2) the overall displacement of water from the measurement volume by excess soluble guest. The variance of $\Delta\epsilon_{\text{W}}$ is best described by including the dipole moment of the cargo (Figure 6c). The average number of bound water molecules, thus, appears to depend more on the electrostatic environment of the cage with the guest than on the dynamics of the guest binding.

In ionic solutions, the time constant of the Debye relaxation of water is increased when the hydrogen bonding network is strengthened by larger, structure-making (cosmotropic) species.^{33–37} Cages in solution increase the time constant of the D₂O relaxation, indicating a strengthening of the hydrogen bonding network around the cage and counterion and in the bulk. We tested for but did not observe the presence of a separate bound D₂O Debye relaxation, as reported by others.³⁸ We observed a trend similar to ϵ_{W} , where host-guest complexes of more soluble guests behave the most like cages with no guests, whereas insoluble guests have lower τ_{W} overall, indicating more disruption to the hydrogen bonding network. The variance in τ_{W} is best correlated to the solubility of the cage rather than dipole moment. These two observations combined suggest that the disruption to the hydrogen bonding network we observe is due to the behavior of the guest-loaded cage, rather than the excess guest in solution. One potential explanation is that a guest-containing cage is less flexible and acts as a barrier to the fluctuations of the hydrogen bonding network, and cages with insoluble guests are on average more likely to bind a guest. Determining a clear physical understanding of the chaotropic effect of cages with insoluble cargo would require extensive force-field development and large-scale classical molecular dynamics simulations with complementary experimental results. Such development would usefully add to the understanding of the behavior of these species.

CONCLUSIONS

In this report, we quantified the impact of guests on the solution environment of an Fe^{II}₄L₄ cage with sulfate counterions. By fitting MMS spectra of cages with different guests to equivalent circuit models, we extracted the ionic conductivity and Debye relaxations associated with the cage-counterion pair and the hydrogen bonding network of D₂O. Our measurements demonstrated that guests inside the cage impact the environment of the cage and the physicochemical property that best describes the variance in the spectra is water solubility of the cargo. We emphasize that while the correlations from PCA show great promise, more research would be needed to claim a causal or predictive relationship between our measurements and the chemical properties of the guest. Our work highlights the need to couple microwave microfluidics measurements and improved force fields for supramolecular systems so that we can explicitly account for charge-based, entropic, and solvent effects. Studying ion-pairing and solvation interactions in host-guest complexes is critical to developing design parameters for noncovalent interactions in solution. More generally, we envision MMS as a tool for supramolecular chemists to elucidate intermolecular interactions that are

critical to the behavior of host–guest systems in solution. Solvation and ion pairing interactions are often implicated when supramolecular systems behave unexpectedly, and MMS can be a powerful tool for quantifying these interactions.

■ ASSOCIATED CONTENT

SI Supporting Information

The Supporting Information is available free of charge at <https://pubs.acs.org/doi/10.1021/jacs.3c01409>.

Experimental details, NMR spectra, and description of principal components analysis (PDF)

■ AUTHOR INFORMATION

Corresponding Author

Angela C. Stelson – National Institute of Standards and Technology Communications Technology Laboratory, Boulder, Colorado 80305, United States; orcid.org/0000-0002-8900-140X; Email: angela.stelson@nist.gov

Authors

Hugh P. Ryan – Cambridge University Department of Chemistry, University of Cambridge, Cambridge CB2 1EW, U.K.

Zachary S. Fishman – National Institute of Standards and Technology Communications Technology Laboratory, Boulder, Colorado 80305, United States

Jacob T. Pawlik – National Institute of Standards and Technology Communications Technology Laboratory, Boulder, Colorado 80305, United States

Angela Grommet – Cambridge University Department of Chemistry, University of Cambridge, Cambridge CB2 1EW, U.K.; orcid.org/0000-0002-9858-8556

Malgorzata Musial – National Institute of Standards and Technology Material Measurement Laboratory, Gaithersburg, Maryland 20899, United States

Felix Rizzuto – Cambridge University Department of Chemistry, University of Cambridge, Cambridge CB2 1EW, U.K.; orcid.org/0000-0003-2799-903X

James C. Booth – National Institute of Standards and Technology Communications Technology Laboratory, Boulder, Colorado 80305, United States

Christian J. Long – National Institute of Standards and Technology Communications Technology Laboratory, Boulder, Colorado 80305, United States

Kathleen Schwarz – National Institute of Standards and Technology Material Measurement Laboratory, Gaithersburg, Maryland 20899, United States; orcid.org/0000-0002-1539-4511

Nathan D. Orloff – National Institute of Standards and Technology Communications Technology Laboratory, Boulder, Colorado 80305, United States

Jonathan R. Nitschke – Cambridge University Department of Chemistry, University of Cambridge, Cambridge CB2 1EW, U.K.

Complete contact information is available at:

<https://pubs.acs.org/doi/10.1021/jacs.3c01409>

Author Contributions

The manuscript was written through contributions of all authors. All authors have given approval to the final version of the manuscript. These authors contributed equally.

Funding

This research was supported by the National Research Council Fellowship Program, the NIST-on-a-Chip Initiative, the Materials Genome Initiative, UK Engineering and Physical Sciences Research Council (EPSRC EP/T031603/1) and the European Research Council (ERC 695009). FJR acknowledges support from a Cambridge Australia Scholarship. H.P.R. acknowledges funding from the Cambridge Commonwealth, European and International Trust and Christ's College, University of Cambridge.

Notes

The authors declare no competing financial interest.

■ ACKNOWLEDGMENTS

The authors would like to thank Meagan Papac, Michael Woodcox, Paul Hale, Jeffrey Jargon, and Chris Holloway for their careful review of the manuscript. Certain commercial equipment, instruments, or materials are identified in this paper in order to specify the experimental procedure adequately. Such identification is not intended to imply recommendation or endorsement by the National Institute of Standards and Technology, nor is it intended to imply that the materials or equipment identified are necessarily the best available for the purpose.

■ REFERENCES

- (1) Chakrabarty, R.; Mukherjee, P. S.; Stang, P. J. Supramolecular Coordination: Self-Assembly of Finite Two- and Three-Dimensional Ensembles. *Chem. Rev.* **2011**, *111*, 6810–6918.
- (2) Zhang, D.; Ronson, T. K.; Nitschke, J. R. Functional Capsules via Subcomponent Self-Assembly. *Acc. Chem. Res.* **2018**, *51* (10), 2423–2436.
- (3) Smulders, M. M. J.; Zarra, S.; Nitschke, J. R. Quantitative Understanding of Guest Binding Enables the Design of Complex Host-Guest Behavior. *J. Am. Chem. Soc.* **2013**, *135* (18), 7039–7046.
- (4) Turega, S.; Cullen, W.; Whitehead, M.; Hunter, C. A.; Ward, M. D. Mapping the Internal Recognition Surface of an Octanuclear Coordination Cage Using Guest Libraries. *J. Am. Chem. Soc.* **2014**, *136* (23), 8475–8483.
- (5) Cautela, J.; Lattanzi, V.; Månsson, L. K.; Galantini, L.; Crassous, J. J. Sphere - Tubule Superstructures through Supramolecular and Supracolloidal Assembly Pathways. *Small* **2018**, *14*, 1803215.
- (6) Cullen, W.; Metherell, A. J.; Wragg, A. B.; Taylor, C. G. P.; Williams, N. H.; Ward, M. D. Catalysis in a Cationic Coordination Cage Using a Cavity-Bound Guest and Surface-Bound Anions: Inhibition, Activation, and Autocatalysis. *J. Am. Chem. Soc.* **2018**, *140* (8), 2821–2828.
- (7) Fang, Y.; Powell, J. A.; Li, E.; Wang, Q.; Perry, Z.; Kirchon, A.; Yang, X.; Xiao, Z.; Zhu, C.; Zhang, L.; Huang, F.; Zhou, H. C. Catalytic Reactions within the Cavity of Coordination Cages. *Chem. Soc. Rev.* **2019**, *48*, 4707–4730.
- (8) Custelcean, R. Anion Encapsulation and Dynamics in Self-Assembled Coordination Cages. *Chem. Soc. Rev.* **2014**, *43* (6), 1813–1824.
- (9) Grommet, A. B.; Nitschke, J. R. Directed Phase Transfer of an Fe^{II} L₄ Cage and Encapsulated Cargo. *J. Am. Chem. Soc.* **2017**, *139* (6), 2176–2179.
- (10) Percástegui, E. G.; Mosquera, J.; Ronson, T. K.; Plajer, A. J.; Kieffer, M.; Nitschke, J. R. Waterproof Architectures through Subcomponent Self-Assembly. *Chem. Sci.* **2019**, *10* (7), 2006–2018.
- (11) He, J.; Li, H.; Yang, P.; Haso, F.; Wu, J.; Li, T.; Kortz, U.; Liu, T. Tuning of Polyoxopalladate Macroanionic Hydration Shell via Counteranion Interaction. *Chem.—Eur. J.* **2018**, *24* (12), 3052–3057.

- (12) Oleinikova, A.; Sasisanker, P.; Weingärtner, H. What Can Really Be Learned from Dielectric Spectroscopy? A Case Study of Ribonuclease A. *J. Phys. Chem. B* **2004**, *108*, 8467–8474.
- (13) Charkhesht, A.; Regmi, C. K.; Mitchell-Koch, K. R.; Cheng, S.; Vinh, N. Q. High-Precision Megahertz-to-Terahertz Dielectric Spectroscopy of Protein Collective Motions and Hydration Dynamics. *J. Phys. Chem. B* **2018**, *122* (24), 6341–6350.
- (14) Marcus, Y.; Hefter, G. Ion Pairing. *Chem. Rev.* **2006**, *106* (11), 4585–4621.
- (15) Vinh, N. Q.; Sherwin, M. S.; Allen, S. J.; George, D. K.; Rahmani, A. J.; Plaxco, K. W. High-Precision Gigahertz-to-Terahertz Spectroscopy of Aqueous Salt Solutions as a Probe of the Femtosecond-to-Picosecond Dynamics of Liquid Water. *J. Chem. Phys.* **2015**, *142* (16), 164502.
- (16) Riedel, R.; Seel, A. G.; Malko, D.; Miller, D. P.; Sperling, B. T.; Choi, H.; Headen, T. F.; Zurek, E.; Porch, A.; Kucernak, A.; Pyper, N. C.; Edwards, P. P.; Barrett, A. G. M. Superalkali-Alkalide Interactions and Ion Pairing in Low-Polarity Solvents. *J. Am. Chem. Soc.* **2021**, *143* (10), 3934–3943.
- (17) Stelson, A. C.; Hong, C. M.; Groenenboom, M. C.; Little, C. A. E.; Booth, J. C.; Orloff, N. D.; Bergman, R. G.; Raymond, K. N.; Schwarz, K. A.; Toste, F. D.; Long, C. J. Measuring Ion-Pairing and Hydration in Variable Charge Supramolecular Cages with Microwave Microfluidics. *Commun. Chem.* **2019**, *2* (1), 54.
- (18) Bolliger, J. L.; Ronson, T. K.; Ogawa, M.; Nitschke, J. R. Solvent Effects upon Guest Binding and Dynamics of a FeII₄L₄ Cage. *J. Am. Chem. Soc.* **2014**, *136* (41), 14545–14553.
- (19) Buchner, R.; Hefter, G. Interactions and Dynamics in Electrolyte Solutions by Dielectric Spectroscopy. *Phys. Chem. Chem. Phys.* **2009**, *11* (40), 8984.
- (20) Little, C. A. E.; Orloff, N. D.; Hanemann, I. E.; Long, C. J.; Bright, V. M.; Booth, J. C. Modeling Electrical Double-Layer Effects for Microfluidic Impedance Spectroscopy from 100 kHz to 110 GHz. *Lab Chip* **2017**, *17* (15), 2674–2681.
- (21) York, D.; Evensen, N. M.; Martinez, M. L.; de Basabe Delgado, J. Unified Equations for the Slope, Intercept, and Standard Errors of the Best Straight Line. *Am. J. Phys.* **2004**, *72* (3), 367–375.
- (22) Pham, D. N. K.; Roy, M.; Kreider-Mueller, A.; Golen, J. A.; Manke, D. R. The crystal structures of iron and cobalt pyridine (py)–sulfates, [Fe(SO₄)(py)₄] and [Co₃(SO₄)₃(py)₁₁]. *Acta Crystallogr., Sect. E: Crystallogr. Commun.* **2018**, *74*, 857–861.
- (23) Popov, I.; Ishai, P. B.; Khamzin, A.; Feldman, Y. The Mechanism of the Dielectric Relaxation in Water. *Phys. Chem. Chem. Phys.* **2016**, *18* (20), 13941–13953.
- (24) Gekle, S.; Netz, R. R. Anisotropy in the Dielectric Spectrum of Hydration Water and Its Relation to Water Dynamics. *J. Chem. Phys.* **2012**, *137* (10), 104704.
- (25) Rinne, K. F.; Gekle, S.; Bonthuis, D. J.; Netz, R. R. Nanoscale Pumping of Water by AC Electric Fields. *Nanoletters* **2012**, *12*, 1780–1783.
- (26) *Microwave Measurements*; Collier, R., Skinner, D., Eds.; Institution of Engineering and Technology, 2007.
- (27) Buchner, R.; Capewell, S. G.; Hefter, G. T.; May, P. M. Ion-Pair and Solvent Relaxation Processes in Aqueous Na₂SO₄ Solutions. *J. Phys. Chem. B* **1999**, *103* (7), 1185–1192.
- (28) Sebastiani, F.; Bender, T. A.; Pezzotti, S.; Li, W.-L.; Schwaab, G.; Bergman, R. G.; Raymond, K. N.; Dean Toste, F.; Head-Gordon, T.; Havenith, M. An Isolated Water Droplet in the Aqueous Solution of a Supramolecular Tetrahedral Cages. *Proc. Natl. Acad. Sci. U.S.A.* **2020**, *117*, 32954.
- (29) Kaatz, U. Bound Water: Evidence from and Implications for the Dielectric Properties of Aqueous Solutions. *J. Mol. Liq.* **2011**, *162* (3), 105–112.
- (30) Buchner, R.; Barthel, J. Kinetic Processes in the Liquid Phase Studied by High-Frequency Permittivity Measurements. *J. Mol. Liq.* **1995**, *63* (1–2), 55–75.
- (31) Mamatkulov, S. I.; Rinne, K. F.; Buchner, R.; Netz, R. R.; Bonthuis, D. J. Water-Separated Ion Pairs Cause the Slow Dielectric Mode of Magnesium Sulfate Solutions. *J. Chem. Phys.* **2018**, *148* (22), 222812.
- (32) Schrödl, S.; Wachter, W.; Buchner, R.; Hefter, G. Scandium Sulfate Complexation in Aqueous Solution by Dielectric Relaxation Spectroscopy. *Inorg. Chem.* **2008**, *47* (19), 8619–8628.
- (33) Wachter, W.; Kunz, W.; Buchner, R.; Hefter, G.; Regensburg, D.; Hefter, G.; Dse, C.; V, M. U. Is There an Anionic Hofmeister Effect on Water Dynamic? Dielectric Spectroscopy of Aqueous Solutions of NaBr, NaI, NaNO₃, and NaSCN. *J. Phys. Chem. A* **2005**, *109*, 8675–8683.
- (34) Marcus, Y. Effect of Ions on the Structure of Water: Structure Making and Breaking. *Chem. Rev.* **2009**, *109*, 1346–1370.
- (35) Agieienko, V.; Buchner, R. Urea Hydration from Dielectric Relaxation Spectroscopy: Old Findings Confirmed, New Insights Gained. *Phys. Chem. Chem. Phys.* **2016**, *18* (4), 2597–2607.
- (36) Hayashi, Y.; Katsumoto, Y.; Omori, S.; Kishii, N.; Yasuda, A. Liquid Structure of the Urea-Water System Studied by Dielectric Spectroscopy. *J. Phys. Chem. B* **2007**, *111* (5), 1076–1080.
- (37) Hunger, J.; Niedermayer, S.; Buchner, R.; Hefter, G. Are Nanoscale Ion Aggregates Present in Aqueous Solutions of Guanidinium Salts? *J. Phys. Chem. B* **2010**, *114* (43), 13617–13627.
- (38) Singh, A. K.; Wen, C.; Cheng, S.; Vinh, N. Q. Long-Range DNA-Water Interactions. *Biophys. J.* **2021**, *120* (22), 4966–4979.

Recommended by ACS

Beyond Duality: Rationalizing Repulsive Coulomb Barriers in Host–Guest Cyclodextrin–Dodecaborate Complexes

Yanrong Jiang, Xue-Bin Wang, *et al.*

JULY 20, 2023
THE JOURNAL OF PHYSICAL CHEMISTRY LETTERS

READ 

Interrogating Encapsulated Protein Structure within Metal–Organic Frameworks at Elevated Temperature

Rohan Murty, Krista S. Walton, *et al.*

MARCH 24, 2023
JOURNAL OF THE AMERICAN CHEMICAL SOCIETY

READ 

Subtle Stereochemical Effects Influence Binding and Purification Abilities of an Fe^{II}₄L₄ Cage

Weichao Xue, Jonathan R. Nitschke, *et al.*

FEBRUARY 27, 2023
JOURNAL OF THE AMERICAN CHEMICAL SOCIETY

READ 

Mechanical Bond-Assisted Full-Spectrum Investigation of Radical Interactions

Yang Jiao, J. Fraser Stoddart, *et al.*

DECEMBER 12, 2022
JOURNAL OF THE AMERICAN CHEMICAL SOCIETY

READ 

Get More Suggestions >